Effect of sandblasting, annealing and hydrophobic treatment on the nano-mechanical and corrosion behaviour of *n*-TiO_2-coated 316L stainless steel

Zaki Ahmad[1,2], Faheemuddin Patel[2], Naila Riaz Mastoi[1,*] and Ayesha Saddiqa[1]

[1]Department of Chemical Engineering, COMSATS Institute of Information Technology, Lahore, Pakistan
[2]King Fahd University of Petroleum and Minerals, Dhahran, Saudi Arabia

In this article, the effect of hydrophobic coated and uncoated surfaces on the corrosion resistance, tribological property, and surface morphology and nano-mechanical properties is presented. A hierarchical surface (micro/nano) was prepared by ultra shot penning of 316L stainless steel at 20 kHz. Chemical vapour deposition technique was used for deposition of the coating, and coating thickness of 0.5 μm was obtained. A maximum hardness of 6.7 and 6.32 GPa was exhibited by the sandblasted (SB), annealed (SBAT) and coated (SBAT) samples respectively. The beneficial effect of annealing and surface roughness was clearly indicated by the sandblasted, annealed and coated specimens. They showed the highest value of reduced modulus maximum resistance to scratch tests and a high adhesion as indicated by scratch path profiles. The lowest corrosion rates were obtained by SBAT specimens (1.32 mpy) in 3.5 wt% NaCl. After application of 3.5% fluoroalkylsilane (FAS13), the corrosion rate was reduced to 0.04 mpy with no evidence of localized pitting. The water contact angle using DSA-100 system was measured to be 120° for SBAT and 80–90° for the samples.

Keywords: Annealing, chemical vapour deposition, corrosion, sandblasting, super hydrophobicity.

ONE of the most striking achievements in the past decade is the dramatic shift in focus of engineers and scientists on fabrication of novel surfaces with unique properties such as high resistance to corrosion wear, fatigue and scratch with embedded hydrophilicity and hydrophobicity. This comes from nature which has already developed an elegant approach that combines physics, chemistry and materials science to create water and dust-repellent surfaces – lotus leaves are the perfect example of cleaning phenomena by nature. The leaves remain spotless despite being exposed to dirty environment. Water drops roll around the leaves and carry away the dust from the substrate[1,2]. In recent years, several attempts have been made to mimic the surface of lotus on engineered surfaces. Wettability is an important phenomenon that changes the surface properties and its reaction which surface results in improvement of substrate properties[3]. Moisture, water, humidity, dust and pollution, all lead to erosion and corrosion of the engineered surfaces resulting in direct and indirect losses amounting to billions of dollars and wastage of material resources. The surface properties of water striders, lotus flower, desert beetles and other biological creatures are now being mimicked to create engineered surfaces. The phenomenon of water repellency has motivated a large body of biomimetics effort to increase the hydrophobicity of surfaces[4]. The most important physical phenomenon involving exchange of energy and/or signal transmission takes place on the surfaces of materials. The advances in surface engineering are therefore a consequence of deeper knowledge of how surfaces influence the mechanism and kinetics of this energy and signal transfer. The understanding of surface phenomena at micro and nanometre level has played a key role in development of electronics, information technology, energy, optics, tribology, biology, biomimetics and a rush towards miniaturization. In recent years, hydrophobicity has been used to improve micro-mechanical, tribological and opto-electronic properties[5–7]. Hydrophobic surfaces have been used to combat corrosion and bio-fouling[8,9]. Corrosion costs about 3.5% of the GNP and bio-fouling drastically enhances fuel consumption and marine fouling. Before giving the details of the study based on the effect of hydrophobicity on mechanical properties and corrosion resistance, the phenomenon of wettability is summarized below.

The contact angle θ of a water drop is related to the interfacial energies acting between the solid–liquid (Z_{SL}), solid–vapour (Z_{SV}) and liquid–vapour (Z_{LV}) interfaces (Figure 1) via

$$\cos(\phi) = \frac{V_{SV} - V_{SL}}{V_{LV}}, \quad (1)$$

*For correspondence. (e-mail: nailariaz@ciitlahore.edu.pk)

Equation (1), however, applies to smooth surfaces only. A real surface exhibits two water contact angles: ϕ_{ADV}, the advancing angle, and ϕ_{Rec}, the receding angle. The difference between the two is called contact angle hysteresis (CAH). If ϕ is <90%, it is called hydrophilic and if >90%, it is called hydrophobic. A surface exhibiting $\phi > 150°$ is called super hydrophobic; the super hydrophobicity increases with decreasing surface energy of solid–air interface γ_V. Two different surface regimes can be expected. In the Wenzel regime[10], the liquid wets the surface but the contact angle differs from the true angle.

$$\cos(\theta) = R \cdot \cos(\phi) = R\frac{\gamma_{SV} - \gamma_{SL}}{\gamma_{LV}}, \quad (2)$$

where R is the ratio between the actual surface area and projected apparent area. When the surface comprises of small protrusions which are filled by air, the wettability is considered to be in the Cassie regime. It is described as

$$\cos(\phi°) = -1 + \phi_S[\cos(\phi) + 1]$$

$$= -1 + \phi_S\left[\frac{\gamma_{SV} - \gamma_{SL}}{\gamma_{LV}}\right]. \quad (3)$$

In eq. (3), $(1 - \phi)$ is remaining fraction area of the surface. The water contact angle for a rough surface is greater due to its roughness. On a rough surface water spreads less to decrease the contact area. Water is in complete contact with the solid surface (called Wenzel state). Wenzel suggested that the surface area increases as surface becomes rough. Hence, water would tend to spread more on a rough, hydrophilic surface, while it would spread less on a rough hydrophobic surface to decrease the contact area of the solid. The relationship between the apparent contact angle (ϕ_{rough}) and intrinsic contact angle is described by the Wenzel equation:

$$\cos\phi_{rough} = \gamma\cos\phi_{flat}, \quad (4)$$

where γ is the roughness factor. As $\gamma > 1$ for a rough surface, hence if $\phi_{flat} > 90°$, and if $\phi_{flat} < 90°$, $\phi_{rough} > 90°$, $\phi_{rough} < \phi_{flat}$. Hence in Wenzel states, a hydrophobic surface would become more hydrophobic with an increase in roughness; it is not possible for water to be in complete contact due to its higher energy state. Instead, air may be entrapped between water and the surface, which is a composite surface of solid and air. This state is called Cassie–Baxter state[11] and is given by

$$\cos\phi_{rough} = \phi_{sflat} + \phi_V\cos\phi_{LV} = \phi_S\phi_{fKL} - (1 - \phi_S), \quad (5)$$

where ϕ_S and ϕ_V are fractions of solid and air contacting the water ($\phi_S + \phi_V = 1$). As the contact angle of water on air (ϕ_{LV}) is 180° ($\cos\phi_V = -1$), the increase of ϕ_S results in increase of ϕ_{rough} and a super hydrophobic state would be established.

The relationship between super hydrophobic surfaces and nano coatings using sol–gel technique has been studied on 316L stainless steel[12]. In the study the substrate of 316L stainless steel was coated by *n*-TiO_2 using chemical vapour deposition (CVD) and treated with perfluoroalkyl silane to make the surface hydrophobic. Previous work on *n*-TiO_2 coated and treated with a silane did not report its effect on nano-mechanical properties and surface morphology. The role of surface roughness was not completely elucidated.

The first super water and oil-repellent surface was developed on anodized aluminum[13]. All active metals like zinc, aluminum, steel, iron, etc. corrode when exposed to water and alkaline or acidic solutions in saline aqueous solutions[14,15]. The effect of surface wetting is dependent on surface roughness and low surface energy. A rough surface may be obtained by sandblasting, anodizing or etching. The effect of important factors such as sandblasting, annealing, hydrophobic coating and coating on the nano-mechanical and corrosion resistance of steel coated with a hydrophobic surface is presented in this article.

Experimental procedures

Materials

In the present study, 316L stainless steel plates of 12 mm thickness were used. Table 1 shows the sample designation and conditions.

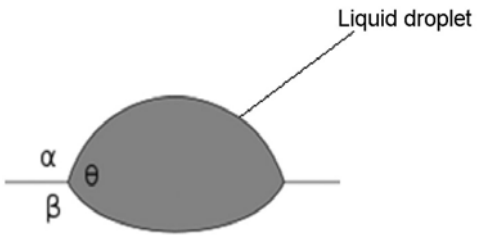

Figure 1. Different fluid phases in mutual contact. α, β and θ represent vapour, solid and liquid phases and their contact angles.

Table 1. Conditions of samples studied

Sample designation	Sample condition
ASR	As received
ASRT	As received–titania-coated
SB	Sandblasted
SBT	Sandblasted–titania coated
SBA	Sandblasted–annealed
SBAT	Sandblasted–annealed–titania-coated and treated with FAS

Nano impact testing

It is a unique technique which allows one to use the high strain rate behaviour of different substrates of material. A micro-material nano-indenter package was used in the study. On impressing a probe onto the surface, the depth signal is continuously monitored. The following were the general testing characteristics. The accelerating load and the probe were accelerated towards the sample from 7.5 μm. The probe used was a 4.3 μm tip radius diamond sphere. Each test comprised of 4 sec cycle and run for 5 min, followed by repetition 6 times.

Nano-mechanical testing

All tests were conducted with a Micro-material nano-indenter (Berkovich Indenter). The nano test loading also allows indentation scratch and impact measurements. The parameters for nano-mechanical testing are as follows: maximum load, 10 min; loading time, 30 sec; dwell period at max level, 10 sec; and unloading time, 30 sec.

Grids of nano-indentations were read on samples. Individual indentation locations were selected using the integrated microscope on all samples.

The effect of sandblasting on grain size is important. Sandblasting has been used as one of the techniques to generate nanostructured grains. The medium used was silica sand (16 μm diameter). Treatment of stainless steel was carried at 240 kPa for 10 sec; keeping the sandblasting nozzle perpendicular to the substrate at 10 cm distance, produced nanostructured grains[16,17]. The measurement of hardness and elastic modulus was introduced in 1992 by nano-indentation[18].

Nano-indentation has facilitated measurement at nano/micro scale. This is now a primary technique for determining the mechanical properties at nano and micro scale. The equipment provides indentation, scratch and impact measurement. The hardness and elastic modulus are measured from indentation load–displacement data obtained during the cycle of loading and unloading. After the contact area is determined, hardness is estimated from:

$$H = \frac{P_{\max}}{A}, \tag{6}$$

where P is the load. The effective elastic modulus is defined by

$$\frac{1}{E_{\text{eff}}} = \frac{1-\gamma^2}{E} + \frac{1-\gamma_1^2}{E_1}, \tag{7}$$

where γ is the Poisson ratio, E the Young's modulus and E_1 the elastic constant. The above were the parameters for loading.

Scratch testing

Scratch testing was done using micromaterials scratch test module[19]. For scratch testing a diamond nano-indenter (10 μm) was used. Following are the parameters: scratch length = 500 μm; maximum load = 100 MN; topography load = 0.01 MN; and loading rate = 2.25 NM/s. Figure 2 shows the scans.

Grain size measurement

Grain size was determined by topographic imaging using AFM (Nano-R2 AFM) equipped with a centi-lever scanner. The grain size is measured in phase imaging, when an oscillatory centi-lever scans the sample surface and the tip of sample is fixed through a feedback loop. Contrast is measured by phase angles. The data are combined simultaneously with topographic data to obtain grain size and its distribution. Topography of 1.47×1.47 μm shows nano-grains.

Fabrication of hierarchical surfaces

The surface of 316L stainless steel was polished with 600-grit paper and sandblasted by a flow of silica particles of 50–70 mesh under a pressure of 200 KPa for 10 min. After sandblasting, the sample was annealed at 35°C for 60 min. The surface was polished with 1 μm diamond paste to maintain consistent roughness. A grain size of 37 nm was obtained. The grain size showed an increase with increase in depth and reached about 100 nm in the transition zone adjacent to the unaffected inner layer.

Treatment of sample

After coating with TiO_2, the samples were treated in a methanol solution of perflouro silane. The specimens were finally dried for 4 h at 105°C. Before CVD coating

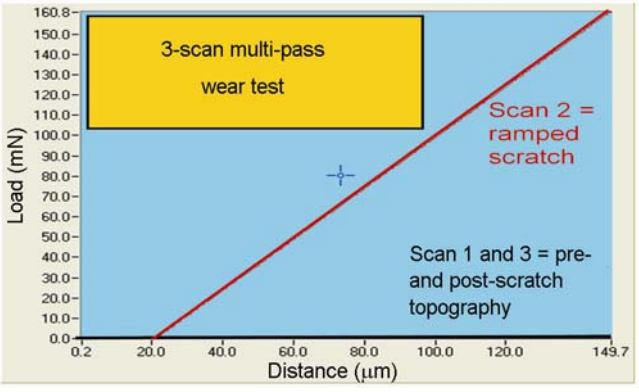

Figure 2. Topographic scan made prior to scratched testing.

the samples were polished with 600-grade sand paper and sandblasting by a flow of silica particles of 50–70 mesh. A grain size of 20 nm was maintained.

Chemical vapour deposition of TiO_2

A piece of bare stainless steel, 20 mm in diameter and 4 mm in thickness was coated with TiO_2. After being polished with 6 μm diamond paste the sample was finally polished with 0.05 μm γ-alumina using distilled water as lubricant followed by cleaning with acetone, rinsing with deionized water and drying. A thermocouple was attached to a graphite susceptor to monitor the temperature in the vacuum chamber. Titanium isopropoxide was used as a precursor and introduced in the chamber. The sample was heated to 53°C. The applied voltage was 480 V, frequency 8 kHz and pressure 4 mbar. The hydrogen flow rate was 200 sec. The plasma assisted chemical vapour deposition (PACVD) process was used to obtain a greater uniformity of coating.

Imaging

The surface morphology of corroded surface was examined by low vacuum electron microscope (LV-SEM filter attached with an EDS system, 100 kV). For topographical studies, an AFM was utilized. Some specimens were also examined under low-vacuum technical field emission gun scanning electron microscope (FEG-SEM).

Water contact angle measurements

A DSA 100 standard frame module was used to measure the wet contact angle. It comprised of two major components; needle and dispensing system. The system projects optical illumination and eliminates optical interference. The evaluation of drop images takes place in a wide window of the software. Contact angles were measured by producing a drop of size 3.5 μl and positioning the needle at the centre of the drop just above the substrate. A high-speed image camera captured the images of the drops and the contact angle and surface tension were calculated using the software Drop Shape Analyzer.

Water and dust repellency testing

Tests on water and dust repellency were conducted with a modified version of ASTM for dirt[20]. A mixture of charcoal and red iron oxide was applied at equidistant points on samples inclined at 45° to the ground. The mixture was left covered with water for 48 h. The slurry was rinsed with water and allowed to dry for 6 h.

Corrosion testing

Corrosion testing included cyclic polarization measurement tests conducted in accordance with ASTM designated standard reference test method[21]. The scanning rate was maintained at 10 mV/min. The protection potential (E_{pp}) was measured by the intersection of forward and reverse polarization curves. Immersion tests to detect loss of weight were performed in accordance with ASTM standard practice for laboratory[22].

Salt spray testing

The specimens were exposed to salt spray test using ASTM standard practice[23]. The resistance of coating to hot and humid environments is best shown by salt spray chamber studies. The enhancement of corrosion resistance is shown by SBT and SBAT specimens, confirming the combined effect of sandblasting, annealing, coating and hydrophobic treatment for corrosion enhancement. The minimal corrosion exhibited by SBT and SBAT confirms the above observations.

Micro structure examination of corrode surface

The specimens were examined under a Philips TECHNT FEG-SEM with a 1.8 nm resolution controller. The focus range was 0.5–0.9 mm and beam current was 1000 nA.

Results and discussion

Nano-indentation studies

The loading–unloading curves are used to determine hardness and Young modulus (Figure 3). A maximum hardness of 6.7 GPa followed by 6.32 GPa is shown by samples SBAT and SBA respectively. Sandblasting gave

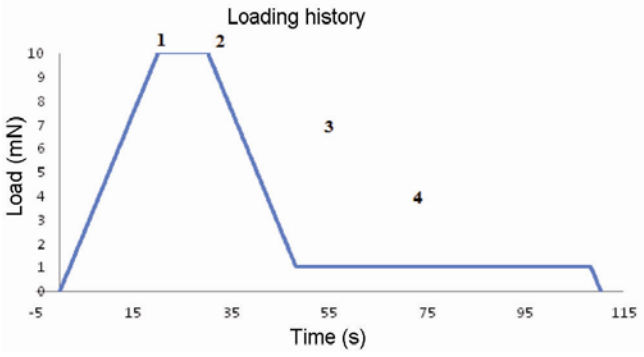

Figure 3. Nano-indentation loading-history curve. Step 1: Loading. Step 2: Max load dwell (creep properties). Step 3: Unloading (used for H and Er calculation). Step 4: Constant load hold for thermal drift measurement.

Table 2. Hardness and reduced modulus results

Sample specifications	Hardness (GPa)	Reduced modulus (GPa)
As received (AR)	5.01 ± 0.35	20.6 ± 11
As received and titania-coated (ART)	4.30 ± 0.33	173.2 ± 12
Sandblasted (SB)	5.98 ± 0.30	216 ± 13.2
Sandblasted and annealed (SBA)	6.32 ± 0.22	214.7 ± 0.81
Sandblasted and titania-coated (SBT)	6.61 ± 0.58	410 ± 7.4
Sandblasted, annealed, titania-coated and hydrophobically treated (SBAT)	6.72 ± 0.24	187 ± 5.3

Table 3. Experimental conditions of scratch tests

Indenter	10 μm diamond
Scratch length	500 μm
Maximum load	100 mN
Loading rate	2.25 mN/S
Load applied after	50 μm
Topography load	0.01 mN
Signals monitored	Depth, load, friction

Table 4. Important electrochemical parameters

	AR	SB	SBAT
EI (mV)	–293.3	–381.4	257.9
I_{corr} (nA)	–142.3	427.4	75.07
R_p (k.Ohm)	152.6	50.8	289.3

10% increase in hardness. Sandblasting increases the surface roughness and reduces the modulus as shown by as received (AR) and sandblasted annealed (SBA). The high ratio of film thickness to surface roughness of the sandblasting sample made scratch testing more difficult. The SB samples enhanced hardness by 10% and elastic modulus by 3%. The titanium coating on untreated samples returned hardness values in good agreement with the literature.

All samples exposed to different conditions listed in Table 2 were subjected to mechanical testing samples. The results obtained from hardness measurements and modulus measurements are described in table. It is observed that sand blasting leads to increased hardness. The highest hardness is shown by SBAT sample. The annealing influences hardness as shown as observed by a significant increase in all specimens subjected to annealing compared to their un-annealed counterpart.

It may be attributed to the even distribution of chromium carbide; however, there is no conclusive evidence. Sand blasting increases surface roughness. As observed by AFM studies, the pile up region caused by indentation extends about 4 μm from the sides of 200 mN indentation. The beneficial effect of sand blasting on crack propagation and fracture is discussed.

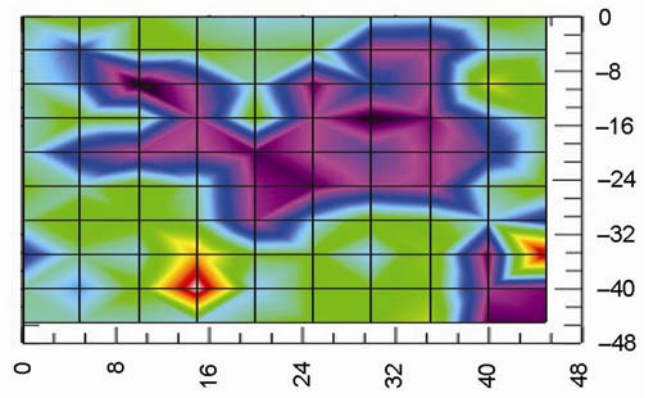

Figure 4. Elastic recover parameter map of SBAT.

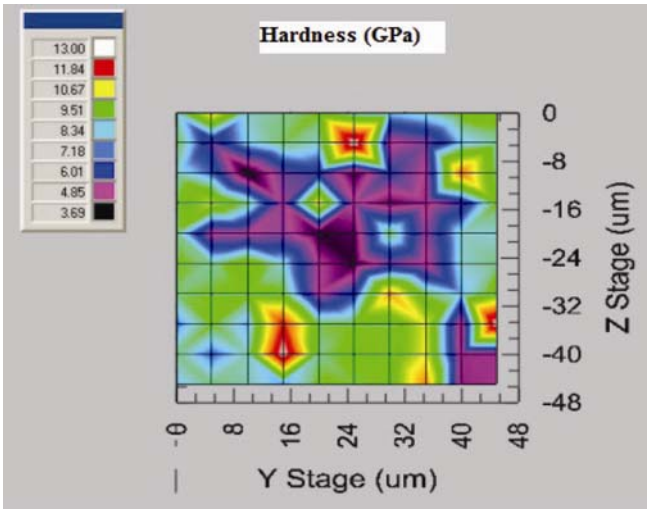

Figure 5. Hardness map of SBAT.

The elastic recovery parameter (ERP) E_r is important and is related to Young modulus of the sample materials E_s by

$$\frac{1}{E_r} = \frac{C_1 - V_s^2}{E_s} + \frac{1 + V_i^2}{E_i}. \quad (8)$$

A depth vs time chart is constructed to determine time-dependent properties. The effect of annealing on enhanced

mechanical strength may be attributed to the formation of a fine precipitate of chromium carbide. However, the specific observation is not well understood. Both the ERP and hardness maps show similar trends (Figure 4). The hardness map shows similar features as the ERP map. Region of lower hardness shows less elastic recovery. It may be noted that the reduced modules map does not show the same spatial variations as hardness and ERP (Figure 5). Inclusions play an important role. As shown by the AFM image an inclusion is observed at the centre. The region around the inclusion displays a significantly lower hardness and elasticity than the surrounding material.

Scratch testing

It is of utmost importance to check the integrity of coating against mechanical damage erosion, abrasion and fracture. Table 3 shows the loading parameters of the scratch test. All un-blasted samples show failure as depicted by depth–time traces. Maximum depth exceeded 3.5 μm. The same observation was exhibited by SBT samples. No evidence of failure was found in sandblasted and annealed specimen. Figures 6 and 7 show the effect of annealing on adhesion and de-lamination of TiO_2 coating. Crack propagation is not observed in SBAT, whereas it is clearly observed in SBT. It shows the rate of annealing which resists crack propagation. The coatings have a better resistance to de-lamination and adhesion in areas directly affected by sandblasting due to increased roughness: The depth and friction data show the failure point in the figures. The friction coefficient is found to be low (0.1). Depth and time curves suggest no evidence of de-lamination in SBAT, in contrast with SBT that shows de-lamination. Figures 8 and 9 show the depth–time curves for SBT and SBAT respectively. The beneficial effect of sandblasting is clearly shown by the above studies.

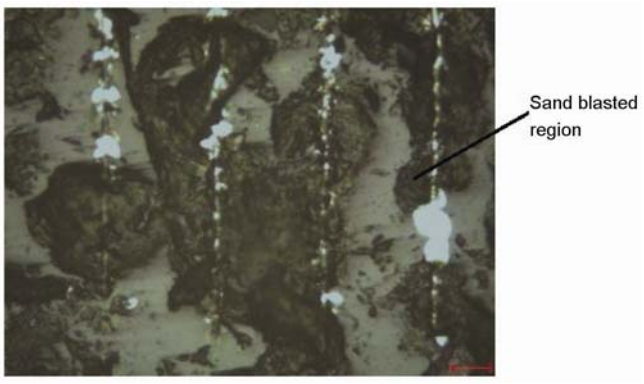

Figure 6. Scratch profile SBT sample.

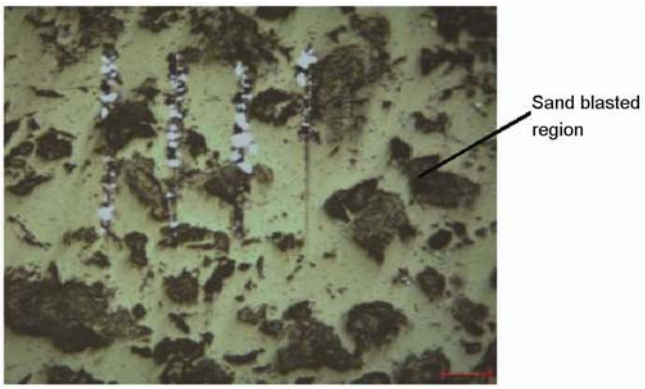

Figure 7. Scratch profile SBAT sample.

Corrosion studies

Corrosion studies made on hydrophobic surfaces have indicated an enhanced resistance to corrosion due to the barrier caused by hydrophobic nano-coating for the penetration of water. Different silanes are used to make a surface hydrophobic. Studies were conducted to observe the effect of hydrophobic surfaces on corrosion resistance of 316L stainless steel. Table 4 shows the results of electrochemical studies and Table 5 shows the results of

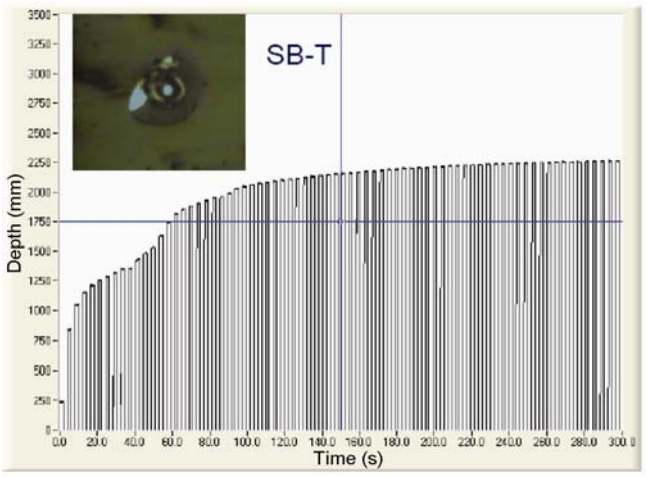

Figure 8. Depth time curves and micrograph of SBT sample.

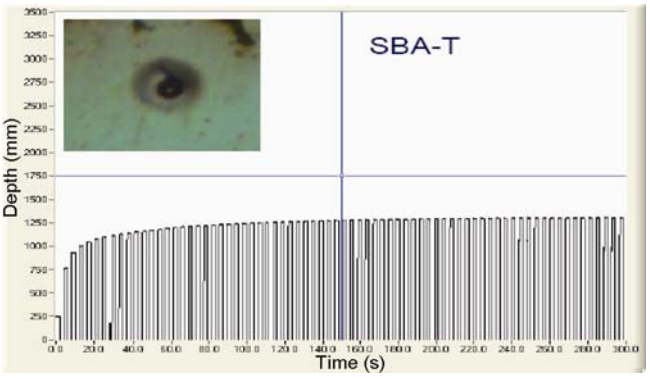

Figure 9. Depth time curves and micrograph of SBAT sample.

Table 5. Corrosion rate of different samples after immersion test

Specimen designation			Corrosion rate (mpy) in 3.5 wt% NaCl			
Time (h)	50	100	150	200	250	300
AR	4.75	4.63	4.0	3.8	3.6	3.5
SB	2.3	2.28	2.1	2.0	1.82	1.92
SBA	2.15	2.10	1.99	1.87	1.79	1.76
ART	2.75	2.88	2.33	2.15	1.78	1.73
SBT	1.93	1.90	1.85	1.63	1.33	1.25
SBAT	1.85	1.80	1.73	1.65	1.4	1.32

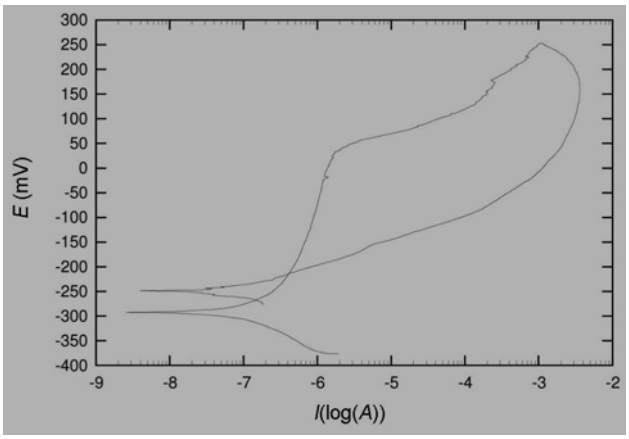

Figure 10. Potentiodynamic cyclic polarization curve for ASR (As received) in 3.5 wt% NaCl.

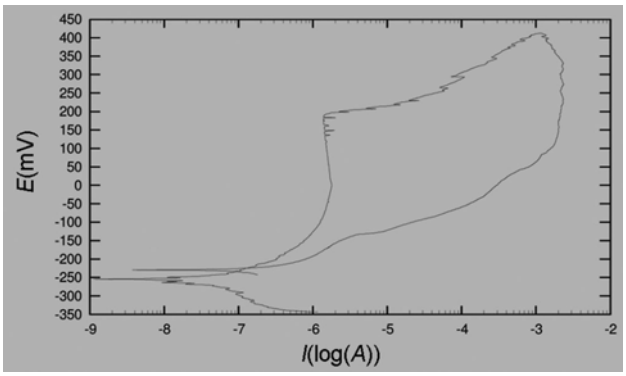

Figure 11. Potentiodynamic cyclic polarization curve for SB (sandblasted) in 3.5 wt% NaCl.

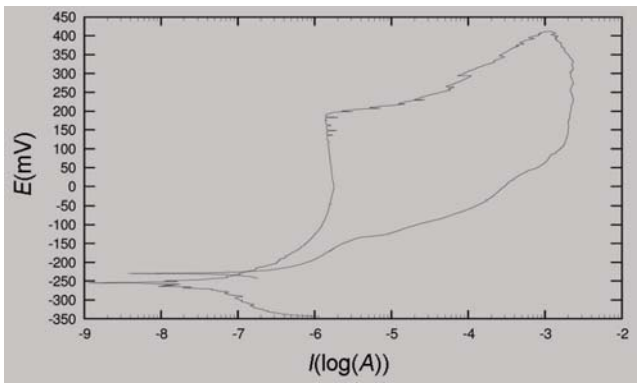

Figure 12. Potentiodynamic cyclic polarization curve for SBA (sandbalsted-annealed) in 3.5 wt% NaCl.

immersion studies. Figures 10–12 show the polarization curves obtained for ASR, SB and SBA in 3.5 wt% NaCl respectively. These studies indicate the beneficial effect which enhances sandblasting and annealing on TiO_2 coated surface enhances the corrosion resistance of 316L stainless steel in 3.5 wt% NaCl. Sandblasting alone, however, decreases the resistance to corrosion as a rough surface and deposition of a low-energy compound are the fundamental requirements to create a hydrophobic surface. Super hydrophobic surface is a porous surface where air is entrapped, and where the accessibility of corrosive species, water and other environmental species is limited. The transportation of oxygen is not influenced by the pores and hence there is no change in the concentration of oxygen in the pores, which may form differential corrosion cells and enhance the dissolution process.

The thickness of the hydrophobic film is uniform over the substrate. The beneficial effect of *n*-TiO_2 coated film and hydrophobic film acts synergistically to increase the corrosion potential (E_{corr}) and decrease the corrosion current (i_{corr}), compared to bare stainless steel (316L). Surface roughness plays a crucial role as it affects cracking of the film. It has been shown that the film does not crack in the sandblast region. Annealing has a positive effect by stabilizing grain boundaries and possible enrichment by chromium. The mechanism is however yet to be understood.

The current I_{corr} decreases from 427.4 nA for SB to 75.07 nA for SBA, and the polarization resistance increased from 50.81 to 289.3 k Ohm (Table 4). Annealing not only causes an enhanced adhesion of the coating on the substrate. But it also creates more uniformity on the surface. Figures 10–12 also show the potentiodynamic polarization curves for the ASR, SB and SBA samples respectively. Upon cyclic polarization, grain boundary attack is clearly observed in 316L stainless steel near E_{pp}. Some pitting adjacent to the grain boundary is also observed. FEG-SEM studies show that SB alone produces dislocation, deformation, corrosion and micro-cracking near E_{pp} (Figure 13). The SBA sample shows a homogeneous grain distribution and a slight grain boundary attack (Figure 14).

The combined effect of sandblasting and annealing is fully revealed in Figure 15, which shows no grain boundary or pitting attack. The enhanced corrosion resistance

may be attributed to the diffusion of chromium to the grain boundary, which extends the passivation range and presents inter-granular corrosion. This also indicates the beneficial effect of the hydrophobic surface on localized corrosion. The substrate forms a Si–O–Si bond and does not allow ingress of water due to treatment with fluoroalkyl silanes (FAS). Micro cracking and inter-granular attack can be observed. In salt spray test, it was observed that the rate of corrosion in general decreased with increased exposure time after an initial increase. The annealed samples show a shift towards minimum corrosion rate after 500 h (Table 6). The above behaviour appears to be dependent on film formation kinetics. A minimum rate of 1.003 mpy was shown by the SBAT sample after hydrophobic treatment with FAS.

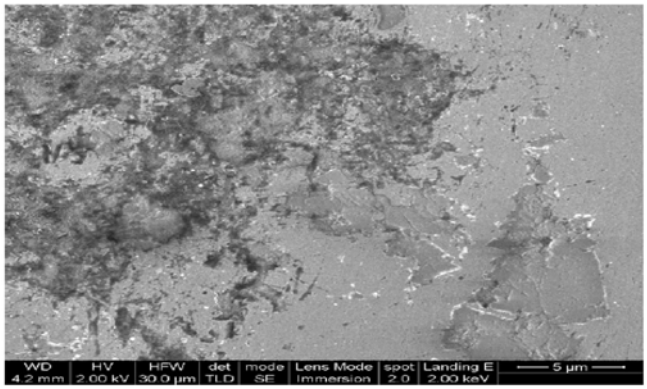

Figure 13. FEG-SEM micrograph of SB sample showing deformation, dislocation, corrosion and slight inter-granular attack after exposure to cyclic polarization in 3.5 wt% NaCl, near E_{pp}.

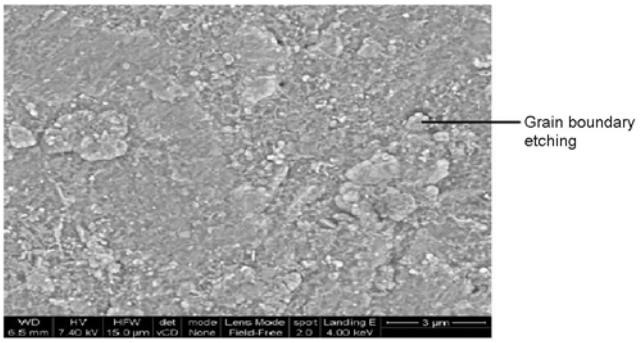

Figure 14. FEG-SEM micrograph of SBA sample showing homogenous grain distribution and slight etching on the grain boundaries after exposure to cyclic polarization in 3.5 wt% NaCl, near E_{pp}.

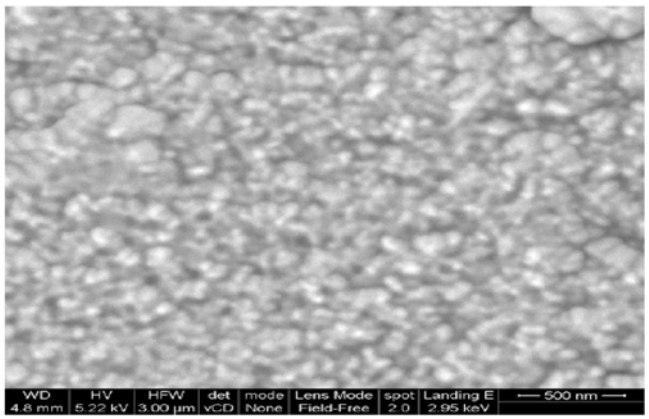

Figure 15. FEG-SEM micrograph of SBAT sample showing no grain boundary attack after exposure to cyclic polarization in 3.5 wt% NaCl, near E_{pp}.

Water and dust repellency

Water being the main ingredient to initiate corrosion, the removal of H_2O and other moisture-bearing species such as dust and particulate contaminants inhibits the corrosion of protected structures. In water repellency tests, it was observed that only a small surface area (1%) was covered with water on SBAT samples. In dust repellency test, no slurry deposition was observed on the surface of SBAT sample, whereas some deposits occurred on the surface of SBT sample. These tests show that hydrophobic treatment of titanium-coated and annealed surface has a significant impact on water repellency. It may be attributed to a stronger bonding of the silanes with the substrates.

Table 6. Exposure results in salt spray chamber

Designation / Exposure time (h)	Corrosion rate (mpy)		
	100	500	1000
AR	2.5443	1.0945	3.1180
SB	4.1035	1.5623	4.5594
SBA	3.0218	1.3020	3.6984
ART	3.0526	1.2323	2.3580
SBT	2.9350	1.5002	2.3222
SBAT	2.8702	1.0033	2.0880

Table 7. Contact angle on different samples

Sample	CA (H_2O)/°
ART	80.9 ± 1.4
SBT	94.0 ± 2
SBAT	135 ± 5.6

Table 8. Surface free energies (SFE) of different samples

Sample	SFE (total)/ mN/m	SFE (dispersive)/ mN/m	SFE (polar)/ mN/m
ART	35.6	26	6.6
SBT	31.6	28.6	3
SBAT	33.0	31.9	1.1

Water contact angle

Table 7 shows the results obtained from static contact angle measurements using DSA 100. The SBA (sand blasted and annealed) samples show a lesser degree of hydrophilicity compared to the AS and SB samples. Figure 16 shows the effect of annealing on wetting behaviour. As observed in Table 7, the highest water contact angle is shown by SBAT (sandblasted titanium coated and treated with FAS). The AS sample shows hydrophilicity, whereas the sandblasted and titanium-coated sample shows a borderline value of hydrophobicity due to surface roughness. It may be mentioned that small surface energy favours hydrophobicity. Sample SBAT which shows a water contact angle of 135°, has a rough surface due to the presence of nano grains of 20 nm diameter. Specimen SBAT without treatment with perflouroalkylsilane shows a hydrophobic angle of 88.6 ± 2 with water.

Table 8 shows the results of surface free energy. Sample ART has higher polar parts of surface energy, which is consistent with the smaller contact angle of the specimen. The lowest polar part of surface energy is shown by the SBAT and SBT samples, which have rough surfaces and relatively higher water contact angle. The overall surface energy varies between 32 and 33 mN/m, and is indeed very small. The surface tension of a drop of water was measured to be 71.32 mN/m, close to the values reported in the literature for steel. The measurement is useful if corrosion is involved. The negative free energy for water displacement indicates hydrophobicity. However, the phenomenon is not well understood. Sufficient experimental evidence has been obtained to show that sandblasting followed by annealing and coating with TiO_2 provides strong bonding between the coating and the substrate. The super hydrophobicity generated by obtaining a nano/micro hybrid surface minimizes corrosion because a tiny fraction of water only comes in contact with the substrate for a short time. The rolling drop also carries the dirt or other contaminants with it. The minimum moisture absorption on the surface minimizes corrosion.

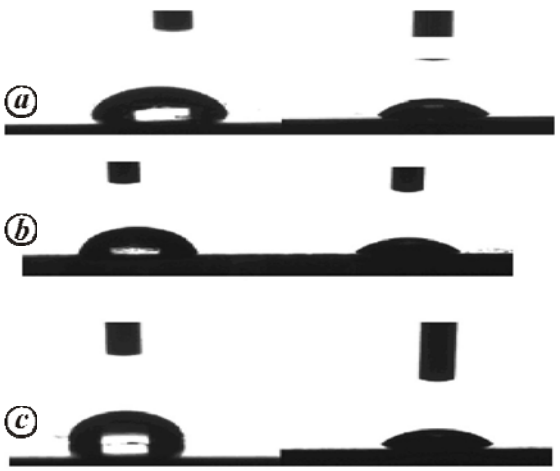

Figure 16. Droplets placed on (***a***) ART (***b***) SBT and (***c***) SBAT samples (left: water; right: di-iodomethane).

Conclusions

The following conclusions are drawn from the present study. The nanostructured hydrophobic surfaces, after sandblasting and annealing, show dramatic improvements in mechanical properties, wear and corrosion resistance. Sandblasting of stainless steel with silica particulates enhances the hardness of steel by 10% and Young modulus by 5%. Sandblasting followed by annealing creates a nano/micro hybrid surface. The hardness and elastic modulii of the samples coated by TiO_2 and annealed are significantly high (55% and 7.5% respectively). TiO_2 coating shows better adhesion in the areas directly affected by sandblasting. No de-lamination occurs in the area of the sandblasting. The water contact angle increases to 135° on applying fluoroalkylsilane. A high resistance to corrosion is observed on exposing the specimen to cyclic polarization, salt spray and immersion testing in 3–5 wt% NaCl. The SBAT sample shows a lower surface energy and high contact angle compared to SBA. Sandblasting has a significant effect on the magnitude of the rough surface, which is a pre-requisite for depositing hydrophobic film. Both annealing and sandblasting have a synergistic effect. Annealing prevents intergranular cracking whereas sandblasting prevents the occurrence of cracks. The TiO_2-coated surface shows good resistance to scratching tests.

The beneficial effect of annealing on corrosion appears to be related to the formation of a fine grain size of an extended passive layer formed due to diffusion of Cr to the grain boundary because of nano-crystallization. The diffusion of Cr by annealing appears to be responsible for the enhancement of nano-mechanical, tribological and corrosion resistance of SBA samples. This is also observed by enhancement of potential in the positive direction. The present study indicates that titanium-coated 316L stainless steel shows improved mechanical properties, scratch and wear and corrosion resistance. Hydrophobicity decreases corrosion, whereas hydrophilicity may have an adverse effect due to its complete contact with the water layer. The synergetic effect of annealing, sandblasting and coating (hydrophobic) enhances the nano-mechanical and corrosion resistance properties of steel. Hence it extends its application potential as well.

1. Barthlott, W. and Neinhuis, C., Purity of the sacred lotus, or escape from contamination in biological surfaces. *Planta*, 1997, **202**, 1–8.

2. Von Bayer, H. C., The lotus-effect. *Science*, 2000, **40**, 12–15.
3. Valipour, M. N, F. Ch. Birjandi and Sargolzaei, J., Super-non-wettable surfaces: a review. *Colloids Surf.*, 2014, **448**, 93–106.
4. Öner, D. and McCarthy, T. J., Ultra hydrophobic surfaces, effects of topography length scales on Wettability. *Langmuir*, 2000, **16**, 7777–7782.
5. Callies, M. and Quere, D., On water repellency. *Soft Mater*, 2005, **1**, 55–65.
6. Xi, Z., Shi, F., Niu, J., Jiaung, Y. and Wang, Z., Super-hydrophobic surface from structural to functional applications. *J. Mater. Chem.*, 2008, **18**, 621–623.
7. Mahaduk Satish, A. *et al.*, Thermally stable and transparent super hydrophobic sol–gel coatings by spray methods. *J. Sol–Gel Sci. Technol.*, 2012, **63**, 580–586.
8. Shen G. X., Chen, Y. C., Lin, L., Lin, C. J. and Scantlebnry, D., Study on hydrophobic Nano-TiO_2 coating and its properties for corrosion protection, metals. *Electro-chemical. Acta*, 2005, **50**, 5083–5089.
9. Ahmad, M. M., Hashim, M. A., Nabi, F., Ahmad, S. and Thabian, A., Anti-corrosion ability of surfactants, a review. *Int. J. Electrochem. Sci*., 2011, **8**, 1927–1948.
10. Wenzel, R. M., Resistance of solid surfaces to wetting the water. *Ind. Eng. Chem.*, 1936, **28**, 988–994.
11. Cassie, A. B. D. and Baxter, S., Wettability of porous surface. *Trans. Faraday Sci*., 1944, **90**, 546–551.
12. Barati. N., Fghihi Sani, M. A., Ghasemi, H., Sadeghian, Z. and Mirhosein, S. M. M., Preparation of uniform TiO_2 nano-structure film on 316L stainless steel by sol–gel dip coating. *J. Appl. Surf. Sci*., 2009, **255**, 828–833.
13. Young, T., An essay on the cohesion of fluids. *Philos. Trans. R. Soc. London*, 1805, **95**, 65–87.
14. Yu, D. *et al.*, Corrosion resistance of three-layer super-hydrophobic composite coating on carbon steel in seawater. *Electrochim. Acta*, 2013, **97**, 409–419.
15. Mohamed Adel, M. A, Abdullah, A. M. and Younan, N. A., Corrosion behavior of super-hydrophobic surfaces: a review. *Proc. Arab. J. Chem.*, 2014; doi: 10.1016/j.arabjc.2014.03.006
16. Beckford, S., Zou, M., Micro/nano engineering on stainless steel substrates to produce superhydrophobic surface. *Thin Solid Film*, 2011, **520**, 1520–1524.
17. Chen, L. J., Chen, M., Di Zhou, H. and Chen, J. M., Preparation of superhydrophobic surface on stainless steel. *Appl. Surf. Sci*., 2008, **255**, 3459–3462.
18. Oliver, W. C. and Pharr, G. M., An improved technique for determining hardness and elastic modulus using load and displacement sensing indentation experiments. *J. Mater. Res*., 1992, **7**, 1564–1583.
19. http://www.micromaterials.co.uk/
20. ASTM D3719-00, Standard test method for quantifying dirt collection on coated exterior panels. ASTM International, PA, USA, 2000, www.astm.org
21. ASTM G5-14, Standard reference test method for making potentiodynamic anodic polarization measurements. ASTM International, PA, USA, 2014; www.astm.org
22. ASTM NACE/ASTMG31-12a, Standard Guide for laboratory immersion corrosion testing of metals. ASTM International, PA, USA, 2012; www.astm.org
23. ASTM B117-11, Standard practice for operating salt spray (fog) apparatus. ASTM International, PA, USA, 2011; www.astm.org

Received 18 November 2014; revised accepted 29 September 2015

doi: 10.18520/cs/v110/i3/353-362